Published in final edited form as:
Hum Brain Mapp. 2013 June ; 34(6): 1306–1318. doi:10.1002/hbm.21511.

A Rat Brain MRI Template with Digital Stereotaxic Atlas of Fine Anatomical Delineations in Paxinos Space and its Automated Application in Voxel-Wise Analysis

Binbin Nie[1], **Kewei Chen**[2,3,4,5], **Shujun Zhao**[6], **Junhua Liu**[7,8], **Xiaochun Gu**[7,8], **Qunli Yao**[9], **Jiaojie Hui**[10], **Zhijun Zhang**[10], **Gaojun Teng**[9], **Chunjie Zhao**[7,8], and **Baoci Shan**[1,*]

[1]Key Laboratory of Nuclear Analytical Techniques, Institute of High Energy Physics, Chinese Academy of Sciences, Beijing 100049, China

[2]Banner Alzheimer's Institute, Banner Good Samaritan Positron Emission Tomography Center, Phoenix, Arizona

[3]Department of Mathematics and Statistics, Arizona State University, Tempe, Arizona

[4]Department of Radiology, University of Arizona, Tucson, Arizona

[5]Arizona Alzheimer's Consortium, Phoenix, Arizona

[6]Nuclear Technology and Application Department, Physical Science and Technology College, Zhengzhou University, Zhengzhou 450052, China

[7]Key Laboratory of Developmental Genes and Human Diseases, MOE, School of Medicine, Southeast University, Nanjing 210009, China

[8]Institute of Brain Science, Southeast University, Nanjing 210009, China

[9]Jiangsu Key Lab of Molecule Imaging and Functional Imaging, Medical School of Southeast University, Nanjing 210009, China

[10]School of Clinical Medicine, Southeast University, Nanjing 210009, China

Abstract

This study constructs a rat brain T_2-weighted magnetic resonance imaging template including olfactory bulb and a compatible digital atlas. The atlas contains 624 carefully delineated brain structures based on the newest (2005) edition of rat brain atlas by Paxinos and Watson. An automated procedure, as an SPM toolbox, was introduced for spatially normalizing individual rat brains, conducting statistical analysis and visually localizing the results in the Atlas coordinate space. The brain template/atlas and the procedure were evaluated using functional images between rats with the right side middle cerebral artery occlusion (MCAO) and normal controls. The result shows that the brain region with significant signal decline in the MCAO rats was consistent with the occlusion position.

*Correspondence to: Baoci Shan, Ph.d., Professor, Key Laboratory of Nuclear Analytical Techniques, Institute of High Energy Physics, Chinese Academy of Sciences, Beijing 100049, China. Tel.: +8610-8823-3185. shanbc@ihep.ac.cn.
Binbin Nie and Kewei Chen contributed equally to this article.

Keywords

SD rat brain; MRI imaging analysis; SPM; normalization; location; co-registration

INTRODUCTION

Magnetic resonance imaging (MRI) techniques have been widely used for the investigation of human brain functions and structures in normal and diseased individuals. Most of these studies are performed on a group of subjects, and the data are analyzed voxel-by-voxel after their brain images are spatially normalized to a brain template, such as the MNI (Montreal Neurological Institute) template. The MNI template is an important part of a number of well known neuroimaging computer software packages, among them is SPM (Welcome Department of Cognitive Neurology, London, UK). In addition to conditioning data for voxel-wise statistical analyses over multiple subjects, the availability of the template also makes it feasible for automated anatomical localizations and references since the MNI template is in the stereotaxic coordinate space of the Talairach atlas [Talairach and Tournoux, 1988] system. Moreover, the automatic human brain area indexing is now a common practice [Lancaster et al., 1997; Tzourio-Mazoyer et al., 2002].

Similarly, MRI techniques have also been widely used in animal studies in the recent years. To process the animal imaging data, either existing analytic tools originally introduced for human studies are evaluated and adopted, or new ones are developed. One of such adaptation efforts is to construct the animal brain template in order to use the existing analytic tools for human studies. In the past several years, several animal brain MRI templates have been constructed for mice [Lin et al., 2003; Sawiak et al., 2009], baboons [Black et al., 2001b], macaque [Alexander et al., 2008; Black et al., 2001a], zebra finch [Poirier et al., 2008], and Sprague-Dawley (SD) rats [Schwarz et al., 2006; Schweinhardt et al., 2003].

To our research interest in the current study, we especially note the role that SD rats played in normal and diseased brain studies [Pawela et al., 2008; Schwarz et al., 2006, 2009]. Accordingly, the SD rat brain template construction and data analysis standardization have been long a methodological topic. For example, although with limited sample size of five and all were female animals, Schweinhardt et al. built a first T_2-weighted SD rat brain template [Schweinhardt et al., 2003]. In a later study, Schwarz et al. introduced their MRI T_2-weighted SD rat brain template with tissue classes for pharmacological MRI studies [Schwarz et al., 2006].

We noted that these reported rat brain templates do not include olfactory bulb. Because a close association between olfactory dysfunction and cognitive impairment has been implied in some researches [Devanand et al., 2000; Peters et al., 2003; Schubert et al., 2008], the olfactory bulb is necessary not only for its own studies but also for the cognitive ones.

A brain template alone is incomplete without a brain atlas system offering detailed anatomical information. Therefore, a co-registration step is needed in order to align the template with the atlas. In 2006, Schwarz et al. [2006] report their template together with the

digital rat brain atlas derived from the fourth edition of rat brain stereo-taxic coordinates built by Paxinos and Watson [1998]. In their study, the nine-parameter affine transformation is used to co-register the template with the atlas based on the homologous anatomical features [Schwarz et al., 2006]. However, alternative approaches might be needed to make more adequate template/atlas co-registration using both linear and non-linear deformation.

With the introduction above, it is desirable to make a rat brain MRI template including olfactory bulb and a compatible digital rat brain atlas available for the widely used computer package SPM. The current study is designed (1) to construct an SD rat brain template that includes olfactory bulb; (2) to create a digital rat brain atlas from the 5th edition of the Paxinos and Watson [2005]; and (3) to develop and implement an automated rat brain image analysis toolbox in the widely used SPM. To evaluate the adequacy of our template together with the digital atlas and to examine the toolbox implemented in SPM, we analyze the data from rats with the right side middle cerebral artery occlusion (MCAO) and those without. This toolbox is available by contacting the corresponding author at shanbc@ihep.ac.cn.

MATERIAL AND METHODS

Animals and Data Acquisition

Twenty-one healthy adult SD rats (female, 9; age range, 10–11 week old; weight range, 250–300 g) were used for template construction in this study. In addition, in order to evaluate the used intracranial mask, ten healthy adult SD rats (male, 10; age range, 11–12 week old; weight range, 250–300 g) were used. Furthermore, in order to demonstrate the values and the practical use of the constructed template in voxel-based procedure, data from additional five SD rats with the right side MCAO (male, 5; age range, 10–12 week old; weight range, 180–240 g) and five healthy SD rats (male, 5; age range, 10–12 week old; weight range, 180–240 g) were analyzed. Intraluminal occlusion of the middle cerebral artery (MCA) was accomplished using a modification of the Longa technique [Longa et al., 1989]. This surgical procedure was performed 30 min prior to the MRI acquisition.

During MRI scan, all rats were anesthetized using inhaled isoflurane/O_2 (3% for induction and 1.5–2% for maintenance) and prostrated on a custom-made holder to minimize head motion while respiration was monitored at a rate of 50 breaths per min.

T_2-weighted data for template construction and functional data of MCAO were acquired on a 7.0 T animal MRI scanner (70/16 PharmaScan, Bruker Biospin GmbH, Germany) in Nanjing, using a 38-mm birdcage rat brain quadrature resonator for radiofrequency transmission and receiving. The structural images were obtained with a rapid acquisition with relaxation enhancement (RARE) sequence (RARE factor = 8, repetition time (TR) = 10,493 ms, echo time (TE) = 36 ms, matrix size 256 × 256 × 90, voxel size 0.14 × 0.14 × 0.3 mm^3, no slice gap). For functional cerebrum, images were obtained with an echo planar imaging (EPI) sequence (TR = 850 ms, TE = 25 ms, matrix size 128 × 128 × 15, voxel size 0.3 × 0.3 × 1 mm^3, flip angle 90°, no slice gap, total of 80 volumes) and coplanar T_2-weighted scan was also acquired in addition to the functional data. All the Bruker original images were converted to DICOM format with programs (Paravision 4.0) in the scanner. All experiments were conducted in accordance with the National Institutes of Health Guide for

the Care and Use of Laboratory Animals and were approved by Jiang Su Animal Care and Use Committee.

T_2-weighted data for evaluating the use of the intracranial mask were acquired on a 7 T/20 cm Bruker Biospec animal MRI scanner in Wuhan. The structural images were obtained with a RARE sequence using a volume coil for radio frequency (RF) transmission and a quadrature surface coil for signal detection (RARE factor = 4, TR = 5800 ms, TE = 40 ms, matrix size 512 × 384 × 52, voxel size 0.068 × 0.091 × 0.58 mm^3, no slice gap). All the Bruker original images were converted to DICOM format with programs (Paravision 4.0) in the scanner. All experiments were conducted in accordance with the National Institutes of Health Guide for the Care and Use of Laboratory Animals and were approved by Hubei Animal Care and Use Committee.

Rat Brain Template Construction

Construction of the rat brain template—The rat brain template with the extracranial tissues was created using SPM2 (Welcome Department of Cognitive Neurology, London, UK). All of the 21 images included in this study were inspected and were found equally of high quality in terms of the image contrast, noise level, and resolution. The rat brain template was created recursively by registering [Ashburner and Friston, 1999; Friston et al., 1995; Zhilkin and Alexander 2004] and averaging as described by Lin et al. [2003]. The constructed template is shown in Figure 1A.

Extraction of the canonical brain and creation of an intracranial mask image—The canonical brain was extracted semi-automatically from the template constructed above by the following two steps. Firstly, a rectangular bounding box was used to roughly remove the extracranial tissues in MRIcro [Rorden and Brett, 2000], especially the voxels of Harderian gland. Then, the intracranial portion of the image including the olfactory was extracted based on Otsu's criterion [Gonzalez et al., 2004].

In addition, an intracranial rat brain mask was formed from this canonical brain by assigning 1 for intracranial voxels and 0 for others, as shown in Figure 1B. Thus, after normalizing an individual image to the rat brain template, the intracranial tissues could be conveniently extracted.

Construction of the Digital Rat Brain Atlas From the Paxinos and Watson Atlas

First, the 2D color figures [Paxinos and Watson, 2005], from the anterior part of olfactory bulb (z_{bregma} + 7.56 mm) to the posterior part of cerebellum (z_{bregma} − 15.72 mm), were converted to gray-scale figures. The background of these figures, including the structure labels and coordinate grids, was removed. Then the outline and internal contours were identified and further enhanced and smoothed by image erosion and dilation [Gonzalez et al., 2004]. Moreover, the slice-to-slice realignment was performed.

Each anatomical structure of the brain atlas was given a unique integer as an index. The laterality information was preserved by assigning odd/even integers for right/left corresponding structures. In this study, 624 structures could be identified in the digital atlas. By doing so, the graphical representation of the atlas was now in the form of 3D

tomographic data. Then, the constructed 3D atlas image was interpolated to create a new 98-slice image with a uniform inter-slice separation of 0.24 mm. This final 3D atlas image was saved as SPM2 compatible Analyze 7.5 format and SPM5/SPM8 compatible NIFTI format. With this digital atlas, a structure could be queried by simply reading the voxel index inside the structure. As an example, one slice of this rat brain atlas image (Bregma −4.20 mm) [Paxinos and Watson, 2005] is given in Figure 2. Appendix A lists information on all structures of this slice including their assigned integer image intensity.

Moreover, the 624 anatomical regions were merged into 66 functional ones according to different brain functions by an anatomist and a co-author of this study (JHL). Among them are sensory cortex, visual cortex, and hippocampus. A new set of integer indices was assigned to these 66 functional regions. Integer indices and functionalities for these 66 regions are listed in Appendix B.

In order to co-register the canonical brain with the prepared tomographic atlas, we created a pseudo T_2-weighted MR image from the 3D atlas [Rubins et al., 2003]. For this purpose, the 624 regions were merged into 12 main anatomy structures, which included olfactory bulb, dorsal part of cortex, ventral part of cortex, hippocampi, corpus striatum, thalamus, hypothalamus, mesencephalon, medulla oblongata, cerebellar, corpus callosum, and ventricle. Finally, this pseudo image was further smoothed using an isotropic Gaussian kernel with a FWHM (Full Width Half Maximum) of two voxels to smooth the juncture of the neighboring segmented parts.

The fine 624 anatomical structures or the 66 functional regions can be used for localization of statistical results. And the low-resolution the pseudo T_2-weighted atlas with 12 regions is for co-registration between the intracranial-only rat brain template and the digital atlas.

Co-Registration of the Canonical Brain With the Paxinos and Watson Rat Atlas

The pseudo MRI was chosen as the target image. The SPM intensity-based affine transformation algorithm and subsequent non-linear warping algorithm was employed to co-register the canonical brain with this target atlas image [Friston et al., 2007], and the transformation matrix was saved to standardize statistical results into the Atlas coordinate space.

Data Analysis of Functional Images in SPM With the Constructed Template and Atlas

The analysis of the functional images was performed in both SPM2 and SPM5 separately. Briefly, the functional image series were realigned to each other and co-registered to the T_2 coplanar image. They were then spatially normalized to the rat brain template via the coplanar. After removing the non-brain tissues via the intracranial mask, the functional series were brought to the canonical space and smoothed with a Gaussian kernel of $2 \times 2 \times 4$ mm^3 FWHM.

In order to identify the difference of signals between the rats with MCAO and the healthy controls, voxel-wise two-sample *t*-test [Friston et al., 2007] was performed accounting for global confounds with proportional scaling. Brain regions with signal reductions in MCAO

rats were identified using $P < 0.001$ (uncorrected) for voxel intensities and 50 for cluster-extent.

RESULTS

The Use of Constructed Rat Brain Template and Intracranial Mask Image

To illustrate the successful use of the intracranial mask in removing non-brain tissues automatically, the dataset obtained in Wuhan was used. As this group of data was acquired using surface coil, the image intensity attenuated seriously from dorsal to ventral. Therefore, the voxels beneath the ventral side were cut off in both the rat brain template and individual images. Then the individual images were normalized to the template, and the intracranial mask was used to remove non-brain tissues, both of which could be performed in our modified SPM. The extraction of three randomly chosen rats result is shown in Figure 3. As shown in Figure 3, the intracranial tissue could be extracted successfully by the intracranial mask.

Co-Registration of the Canonical Brain to the Constructed Rat Brain Atlas

The co-registration result between the canonical brain and atlas was qualitatively and quantitatively evaluated in this study. The constructed atlas is overlaid on the co-registered canonical brain (Fig. 4). Three representative anatomical structures, hippocampus, corpus striatum, and ventricle, are selected from the atlas [Nie et al., 2010] and also overlaid on the canonical brain (Fig. 5). Moreover, the hippocampus on the right side is manually traced out on the canonical brain by an experienced rater, blinded to the atlas. Four volumetric and spatial correspondence measures, Jaccard similarity (JS) [Jaccard, 1912; Lin et al., 2003; Murugavel and Sullivan, 2009], the relative error on volume (RV), the proportions of false-positive (FP), and false-negative (FN) [Chupin et al., 2007; Rodionov et al., 2009], were calculated between the atlas-derived and manual-traced hippocampus, and between the whole brain volumes of the atlas and canonical image. The calculated results are given in Table I, and details of these measures are listed in Appendix C.

Data Analysis of Functional Images in SPM With the Constructed Template and Atlas

The SPM2 based statistical results of the five MCAO rats comparing with the five normal controls are shown in Figure 6. Similar results were also obtained in SPM5 and will not be presented. These regions are all related to the right side MCA.

DISCUSSION

In the current study, we constructed and evaluated T_2-weighted brain template, including the whole olfactory bulb. This SD rat brain template was in the widely used Paxinos coordinate space, which is defined by Paxinos and Watson [2005]. Moreover, to make it easy to use in routine analyses, we incorporated the rat brain template together with standard atlas into the SPM package.

It was found that the spatial normalization of individual rat brains to the template space was satisfactory even when image resolutions differed from that of the data used for the template

creation. As exemplified by analyzing the MCAO data, the use of this template in SPM2 or SPM5 was feasible and practical. We note that the imaging contrast differences between the rats with MCAO and normal controls might be due to the effects of stroke, such as inflammation or necrosis.

In addition, one of our primary aims was to make the removal of the extracranial tissue automated. Alternative to the successful automatic cropping method using pulse coupled neural networks (PCNN) by Murugavel and Sullivan [2009], we proposed the use of intracranial-only mask image which was in the same coordinate space with the template. When an individual image was normalized to the template, the extracranial tissue could be simply removed by the intracranial mask. Our results showed this strategy worked satisfactorily.

The central piece of our efforts was to make the Paxinos and Watson's rat brain atlas [Paxinos and Watson, 2005] available in the coordinate space of our MRI template. We adopted the strategy of converting the atlas map into pseudo T_2-weighted images. This allowed us to use the existing co-registration algorithm with the option of affine only or with non-linear warping. We also envision its general applicability in other template/atlas construction studies.

As any other electronically accessible atlas with detailed labeling for human [Talairach and Tournoux, 1988], the availability of the rat brain atlas can provide two convenient services to researchers. First, detailed structure information could be queried either automatically or interactively in statistical parametric mapping analyses, as showcased in this study (Results and Appendix B). This was very helpful for pin-pointing the exact brain locations where the maximal group/condition differences were observed in voxel-wise analysis, as shown in Figure 6. Second, similar as the work described by Schwarz et al. [2006], volume of interest (VOI) could now be defined straightforward, objective, and free of operator bias [Nie et al., 2010].

In demonstrating the adequacy and usefulness of our work, the functional (T_2*-weighted) image series were spatially normalized to the constructed rat brain template via the coplanar T_2 image of each animal. To do that, we first corrected possible movements in the functional time series and co-registered them to the coplanar T_2 data. This procedure has been common for human studies [Friston et al., 2007]. Nevertheless, if coplanar structural image is not a part of the data acquisition protocol, or not available due to any other reason, the procedure above then becomes non-feasible. An alternative and convenient way to analyze the functional images is to make available of a functional rat brain template in the same coordinate space of the T_2-weighted template. The template construction method and co-registration strategy proposed in this study can be extended in establishing the functional MRI template, even the positron emission tomography (PET) and electronic computer X-ray tomography technique (CT) templates.

As a whole-brain unbiased technique, voxel-based morphometry (VBM) technique has been used for characterizing regional gray/white matter concentration or volume differences. The segmentation of the structural images into grey matter (GM), white matter (WM), and

cerebrospinal fluid (CSF) is prerequisite for the VBM procedure [Good et al., 2001; Keller et al., 2004]. Continuing our current work, we are in the process of establishing GM, WM, and CSF prior probability maps for rat brains and will have it reported separately.

In conclusion, we demonstrated the adequacy and practical usefulness of the constructed template in SPM environment together with the corresponding Paxinos and Watson rat brain atlas. We believe it will be helpful to streamline the neuroimaging data analyses for rat brain imaging studies from the pre-processing stage to the reports of the statistical inference results.

Acknowledgments

Contract grant sponsor: National Basic Research Program of China (973 Program); Contract grant numbers: 2007CB512303, 2011CB707802; Contract grant sponsor: National Natural Science Foundation of China; Contract grant number: 30970768; Contract grant sponsor: Tianjin Natural Science Foundation; Contract grant number: 08JCZDJC23700; Contract grant sponsor: National Institute of Mental Health US; Contract grant number: ROI MH57899; Contract grant sponsor: National Institute on Aging, US; Contract grant numbers: 9R01AG031581-10, P30 AG19610; Contract grant sponsor: The state of Arizona.

References

Alexander GE, Chen K, Aschenbrenner M, Merkley TL, Santerre-Lemmon LE, Shamy JL, Skaggs WE, Buonocore MH, Rapp PR, Barnes CA. Age-related regional network of magnetic resonance imaging gray matter in the rhesus macaque. J Neurosci. 2008; 28:2710–2718. [PubMed: 18337400]

Ashburner J, Friston KJ. Nonlinear spatial normalization using basis functions. Hum Brain Mapp. 1999; 7:254–266. [PubMed: 10408769]

Black KJ, Koller JM, Snyder AZ, Perlmutter JS. Template images for nonhuman primate neuroimaging. II. Macaque. NeuroImage. 2001a; 14:744–748. [PubMed: 11506546]

Black KJ, Snyder AZ, Koller JM, Gado MH, Perlmutter JS. Template images for nonhuman primate neuroimaging. I. Baboon. NeuroImage. 2001b; 14:736–743. [PubMed: 11506545]

Chupin M, Mukuna-Bantumbakulu AR, Hasboun D, Bardinet E, Baillet S, Kinkingnehun S, Lemieux L, Dubois B, Garnero L. Anatomically constrained region deformation for the automated segmentation of the hippocampus and the amygdala: Method and validation on controls and patients with Alzheimer's disease. NeuroImage. 2007; 34:996–1019. [PubMed: 17178234]

Devanand DP, Michaels-Marston KS, Liu X, Pelton GH, Padilla M, Marder K, Bell K, Stern Y, Mayeux R. Olfactory deficits in patients with mild cognitive impairment predict Alzheimer's disease at follow-up. Am J Psychiatry. 2000; 157:1399–1405. [PubMed: 10964854]

Friston KJ, Ashburner J, Frith CD, Pline J-B, Heather JD, Frachowiak RSJ. Spatial registration and normalization of images. Hum Brain Mapp. 1995a; 2:89–165.

Friston, KJ.; Ashburner, JT.; Kiebel, SJ.; Nichols, TE.; Penny, WD. Statistical Parametric Mapping: The Analysis of Functional Brain Images. London: Academic Press; 2007.

Gonzalez, RC.; Woods, RE.; Eddins, SL. Digital Image Processing Using MATLAB. Beijing, China: Publishing house of electronics industry; 2004. p. 305-307.

Good CD, Johnsrude IS, Ashburner J, Henson RN, Friston KJ, Frackowiak RS. A voxel-based morphometric study of ageing in 465 normal adult human brains. NeuroImage. 2001; 14(1 Part 1): 21–36. [PubMed: 11525331]

Jaccard P. The distribution of the flora in the alpine zone. New Phytol. 1912; 11:37–50.

Keller SS, Wilke M, Wieshmann UC, Sluming VA, Roberts N. Comparison of standard and optimized voxel-based morphometry for analysis of brain changes associated with temporal lobe epilepsy. NeuroImage. 2004; 23:860–868. [PubMed: 15528086]

Lancaster JL, Rainey LH, Summerlin JL. Automated labeling of the human brain: A preliminary report on the development and evaluation of a forward transform method. Human brain mapping. 1997; 5:1–5. [PubMed: 20408205]

Lin L, Chen K, Alexander GE, He J, Valla J, Galons J-P, Hauss-Wegrzyniak B, Reiman EM. Construction of mouse brain MRI templates using SPM99. Modeling and control in biomedical systems. 2003:113–118.

Longa EZ, Weinstein PR, Carlson S, Cummins R. Reversible middle cerebral artery occlusion without craniectomy in rats. Stroke. 1989; 20:84–91. [PubMed: 2643202]

Murugavel M, Sullivan JM Jr. Automatic cropping of MRI rat brain volumes using pulse coupled neural networks. NeuroImage. 2009; 45:845–854. [PubMed: 19167504]

Nie B, Hui J, Wang L, Chai P, Gao J, Liu S, Zhang Z, Shan B, Zhao S. Automatic method for tracing regions of interest in rat brain magnetic resonance imaging studies. J Magn Reson Imaging. 2010; 32:830–835. [PubMed: 20882613]

Pawela CP, Hudetz AG, Ward BD, Schulte ML, Li R, Kao DS, Mauck MC, Cho YR, Neitz J, Hyde JS. Modeling of region-specific fMRI BOLD neurovascular response functions in rat brain reveals residual differences that correlate with the differences in regional evoked potentials. NeuroImage. 2008; 41:525–534. [PubMed: 18406628]

Paxinos, G.; Watson, C. The Rat Brain in Stereotaxic Coordinates. 4. San Diego: Academic Press; 1998.

Paxinos, G.; Watson, C. The Rat Brain in Stereotaxic Coordinates. 5. New York: Academic Press; 2005.

Peters JM, Hummel T, Kratzsch T, Lotsch J, Skarke C, Frolich L. Olfactory function in mild cognitive impairment and Alzheimer's disease: An investigation using psychophysical and electrophysiological techniques. Am J Psychiatry. 2003; 160:1995–2002. [PubMed: 14594747]

Poirier C, Vellema M, Verhoye M, Van Meir V, Wild JM, Balthazart J, Van Der Linden A. A three-dimensional MRI atlas of the zebra finch brain in stereotaxic coordinates. NeuroImage. 2008; 41:1–6. [PubMed: 18358743]

Rodionov R, Chupin M, Williams E, Hammers A, Kesavadas C, Lemieux L. Evaluation of atlas-based segmentation of hippocampi in healthy humans. Magn Reson Imaging. 2009; 27:1104–1109. [PubMed: 19261422]

Rorden C, Brett M. Stereotaxic display of brain lesions. Behav Neurol. 2000; 12:191–200. [PubMed: 11568431]

Rubins DJ, Melega WP, Lacan G, Way B, Plenevaux A, Luxen A, Cherry SR. Development and evaluation of an automated atlas-based image analysis method for microPET studies of the rat brain. NeuroImage. 2003; 20:2100–2118. [PubMed: 14683714]

Sawiak SJ, Wood NI, Williams GB, Morton AJ, Carpenter TA. Voxel-based morphometry in the R6/2 transgenic mouse reveals differences between genotypes not seen with manual 2D morphometry. Neurobiol Dis. 2009; 33:20–27. [PubMed: 18930824]

Schubert CR, Carmichael LL, Murphy C, Klein BE, Klein R, Cruickshanks KJ. Olfaction and the 5-year incidence of cognitive impairment in an epidemiological study of older adults. J Am Geriatr Soc. 2008; 56:1517–1521. [PubMed: 18662205]

Schwarz AJ, Danckaert A, Reese T, Gozzi A, Paxinos G, Watson C, Merlo-Pich EV, Bifone A. A stereotaxic MRI template set for the rat brain with tissue class distribution maps and co-registered anatomical atlas: Application to pharmacological MRI. NeuroImage. 2006; 32:538–550. [PubMed: 16784876]

Schwarz AJ, Gozzi A, Bifone A. Community structure in networks of functional connectivity: Resolving functional organization in the rat brain with pharmacological MRI. NeuroImage. 2009; 47:302–311. [PubMed: 19345737]

Schweinhardt P, Fransson P, Olson L, Spenger C, Andersson JL. A template for spatial normalisation of MR images of the rat brain. J Neurosci Methods. 2003; 129:105–113. [PubMed: 14511814]

Talairach, P.; Tournoux, J. A Stereotactic Coplanar Atlas of the Human Brain. Stuttgart: Thieme; 1988.

Tzourio-Mazoyer N, Landeau B, Papathanassiou D, Crivello F, Etard O, Delcroix N, Mazoyer B, Joliot M. Automated anatomical labeling of activations in SPM using a macroscopic anatomical parcellation of the MNI MRI single-subject brain. NeuroImage. 2002; 15:273–89. [PubMed: 11771995]

Zhilkin P, Alexander ME. Affine registration: A comparison of several programs. Magn Reson Imaging. 2004; 22:55–66. [PubMed: 14972395]

APPENDIX

APPENDIX A. Detailed information on some of the 624 structures included in the rat atlas by Paxinos and Watson and presented in Figure 2

Index in Figure 5	Structural name	Abbreviation	$Index_L$[a]	$Index_R$[a]
1	Retrosplenial granular cortex, b region	RSGb	178	177
2	Retrosplenial granular cortex, c region	RSGc	156	155
3	Retrosplenial dysgranular cortex	RSD	158	157
4	Senondary visual cortex, mediomedial area	V2MM	184	183
5	Senondary visual cortex, mediolateral area	V2ML	186	185
6	Parietal cortex, posterior area, dorsal part	PtPD	180	179
7	Parietal cortex, posterior area, rostral part	PtPR	190	189
8	Primary somatosensory cortex, barrel field	S1BF	150	149
9	Primary somatosensory cortex	S1	182	181
10	Secondary auditory cortex, dorsal area	AuD	166	165
11	Primary auditory cortex	Au1	168	167
12	Secondary auditory cortex, ventral area	AuV	170	169
13	Ectorhinal cortex	Ect	174	173
14	Perirhinal cortex	PRh	176	175
15	Lateral ectorhinal cortex	LEnt	200	199
16	Piriform cortex	Pir	78	77
17	Dorsal endopiriform nucleus	DEn	94	93
18	Amygdalopiriform transition area	APir	208	207
19	Basolateral amygdaloid nucleus, posterior part	BLP	490	489
20	Amygdalohippocampal area, posterolateral	AHiPL	570	569
21	Amygdalohippocampal area, posteromedial	AHiPM	572	571
22	Posterolateral cortical amygdaloid nucleus	PLCo	686	685
23	Posteromedial cortical amygdaloid nucleus	PMCo	688	687
24	Corpus callosum	cc	930	929
	Cingulum	cg		
	Deep cerebral white matter	dcw		
25	Lateral ventricle	LV	934	933
26	Field CA1 of the hippocampus	CA1	870	869
	Field CA2 of the hippocampus	CA2		
	Field CA3 of the hippocampus	CA3		
	Lacunosum moleculare layer of the hippocampus	LMol		
	Oriens layer of the hippocampus	Or		
	Pyramidal cell layer of the hippocampus	Py		
	Stratum lucidum of the hippocampus	SLu		

Index in Figure 5	Structural name	Abbreviation	$Index_L$[a]	$Index_R$[a]
27	Granular layer of the dentate gyrus	GrDG	982	981
	Polymorph layer of the dentate gyrus	PoDG		
28	Dorsal hippocampal commissure	dhc	1400	1399
	Alveus of the hippocampus	alv		
29	Molecular layer of the dentate gyrus	MoDG	100	99
30	Fimbria of the hippocampus	fi	956	955
31	Lat amygdaloid nucleus	La	976	975
32	Dorsal fornix	df	1078	1077
33	Dorsal 3rd ventricle	D3V	934	933
34	Medial habenular nucleus	MHb	550	549
35	Stria medullaris of the thalamus	sm	605	604
36	Lateral habenular nucleus, medial part	LHbM	552	551
	Lateral habenular nucleus, lateral part	LHbL		
37	Paraventricular thalamic nucleus	PV	2170	2169
38	Centrolateral thalamic nucleus	CL	932	931
39	Lateral posterior thalamic nucleus, mediorostral part	LPMR	556	555
40	Lateral posterior thalamic nucleus, laterorostral part	LPLR	558	557
41	Intramedullary thalamic area	IMA	960	959
42	Dorsal lateral geniculate nucleus	DLG	560	559
43	Intergeniculate leaf	IGL	978	977
44	Ventral lateral geniculate nucleus	VLG	778	777
45	Superior thalamic radiation	str	770	769
46	Optic tract	opt	722	721
47	Subgeniculate nucleus	SubG	952	951
48	Ventral posteromedial thalamic nucleus	VPM	668	667
	Ventral posterolateral thalamic nucleus	VPL		
49	Posterior thalamic nuclear group	Po	554	553
50	Parafascicular thalamic nucleus	PF	546	545
51	Fasciculus retroflexus	fr	548	547
52	Precommissural nucleus	PrC	758	757
53	Periventricular gray	PVG	974	973
54	3rd ventricle	3V	2086	2085
55	A11dopamine cells	A11	452	451
56	Subparafascicular thalamic nucleus	SPF	680	679
	Subparafascicular thalamic nucleus, parvicellular part	SPFPC		
57	Ventral posterior nucleus of the thalamus, parvicellular part	VPPC	682	681
58	Medial lemniscus	ml	866	865
59	Prerubral field	PR	514	513
60	Nucleus of the fields of Forel	F	678	677
61	Zona incerta, dorsal part	ZID	666	665
	Zona incerta, ventral part	ZIV		

Index in Figure 5	Structural name	Abbreviation	$Index_L$[a]	$Index_R$[a]
62	Subthalamic nucleus	STh	676	675
63	Internal capsule	ic	954	953
	Cerebral peduncle	cp		
64	Posterior hypothalamic nucleus	PH	544	543
65	Gemini hypothalamic nucleus	Gem	874	873
66	Submammillothalamic nucleus	SMT	872	871
67	Supramammillary nucleus, medial part	SuMM	762	761
	Supramammillary nucleus, lateral part	SuML		
68	Mammillothalamic tract	mt	454	453
69	Fornix	f	582	581
70	Lateral mammillary nucleus	LM	876	875
71	Medial mammillary nucleus, medial part	MM	772	771
	Medial mammillary nucleus, lateral part	ML		
72	Medial mammillary nucleus, median part	MnM	970	969
73	Mammillary recess of the 3rd ventricle	MRe	972	971
74	Arcuate hypothalamic nucleus, medial posterior part	ArcMP	512	511
	Arcuate hypothalamic nucleus, lateroposterior part	ArcLP		

[a] $Index_L$ is the integer index value for the structure on the left hemisphere. And $Index_R$ is the integer index value for the corresponding structure on the right hemisphere.

APPENDIX B. Detailed information of the 66 structures included in the rat atlas by Paxinos and Watson

Structures				$Index_L$[a]	$Index_R$[a]
Cerebrum	Cerebral cortex	Olfactory bulb		52	51
		Limbic system	Cingulate gyrus	54	53
			Retrosplenial cortex	56	55
			Piriform cortex	58	57
			Bed nucleus of stria terminalis	60	59
			Tenia tecta	62	61
			Septal area	64	63
		Parietal lobe	Parietal cortex posterior area	66	65
			Sensory cortex	68	67
			Parietal association cortex	70	69
		Frontal lobe	Prelimbic cortex	72	71
			Orbital cortex	74	73
			Frontal association cortex	76	75
			Dorsal peduncular cortex	78	77
			Frotal cortex area	80	79

Structures				$Index_L$[a]	$Index_R$[a]
			Infralimbic cortex	82	81
			Motor cortex	84	83
		Occipital lobe	Visual cortex	86	85
		Temporal lobe	Auditory cortex	88	87
		Olfactory cortex	90	89	
		Temporal association cortex	92	91	
		Insular cortex		94	93
	Fiber	Corpus callosum		96	95
		Anterior commissure		98	97
		Posterior commissure		100	99
		Olfactory tract		102	101
	Deep structure	Olfactory tubercle		104	103
		Accumbens nucleus		106	105
		Striatum		108	107
		Amygdaloid body		110	109
		Claustral layer		112	111
		Hippocampus		114	113
		Dentate gyrus		116	115
		Infracerebellar		118	117
		Subthalamic nucleus		120	119
		Substantia nigra		122	121
		Red nucleus		124	123
Interbrain	Dorsal thalamus	Midline nucleus group		126	125
		Anterior nucleus group		128	127
		Medial nucleus group		130	129
		Lateral nucleus group		132	131
	Pineal gland		134	133	
	Hypothalamus	Preoptic region	136	135	
		Supraoptic region	138	137	
		Tuberal region	140	139	
		Mammillary region	142	141	
		Inferior colliculus	144	143	
Cerebellum		Anterior lobel of cerebellum	146	145	
		Posterior lobel of cerebellum	148	147	
		Flocculonodular lobe	150	149	
		Cerebellar nucleus	152	151	
		Interstitial nucleus	154	153	
Brain stem		Medulla oblongata	156	155	
	Pons	Basilar part of pons	158	157	
		Tegmentum of pons	160	159	
	Mesencephalon	Superior colliculus	162	161	

Structures			$Index_L$[a]	$Index_R$[a]
	Inferior colliculus	164	163	
	Tegmentum of midbrain	166	165	
	Cerebral peduncle	168	167	
	Pretectal area	170	169	
	Periaqueductal gray matter	172	171	
Ventricle	3rd ventricle	174	173	
	4th ventricle	176	175	
Blood vessel	Middle cerebral artery	178	177	
	Blood vessel	180	179	
Internal capsule	Capsule	182	181	

[a] $Index_L$ is the integer index value for the structure on the left hemisphere. And $Index_R$ is the integer index value for the corresponding structure on the right hemisphere.

APPENDIX C

The following volumetric and spatial correspondence measures were calculated between the canonical brain ($O_{template}$) and each individual normalized image ($O_{normalized}$):

1. JS = Jaccard similarity as in Eq. (A1) (the optimal value is 100%);

$$JS = \frac{O_{template} \cap O_{normalized}}{O_{template} \cup O_{normalized}} \quad (A1)$$

2. RV = the relative error on volume as in Eq. (A2) (the optimal value is 0%);

$$RV = 2 \cdot \frac{|O_{normalized} - O_{template}|}{O_{normalized} + O_{template}} \quad (A2)$$

3. FP = the proportions of false-positive as in Eq. (A3);

$$FP = \frac{O_{normalized} - (O_{template} \cup O_{normalized})}{O_{template} \cap O_{normalized}} \quad (A3)$$

4. FN = the proportions of false-negative as in Eq. (A4).

$$FN = \frac{O_{template} - (O_{template} \cap O_{normalized})}{O_{template} \cup O_{normalized}} \quad (A4)$$

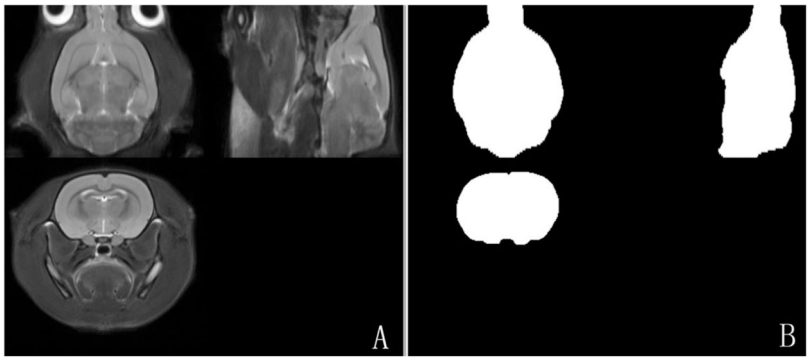

Figure 1.

A: Axial, sagittal and coronal views of the T_2-weighted rat brain template; (**B**) Axial, sagittal and coronal views of the corresponding intracranial mask.

Figure 2.

One slice of the rat brain atlas with detailed anatomical delineation. Note that the integer assigned to each VOI on the figure is not the one designated as the VOI ID. The corresponding VOI ID can be found in Appendix A. [Color figure can be viewed in the online issue, which is available at wileyonlinelibrary.com.]

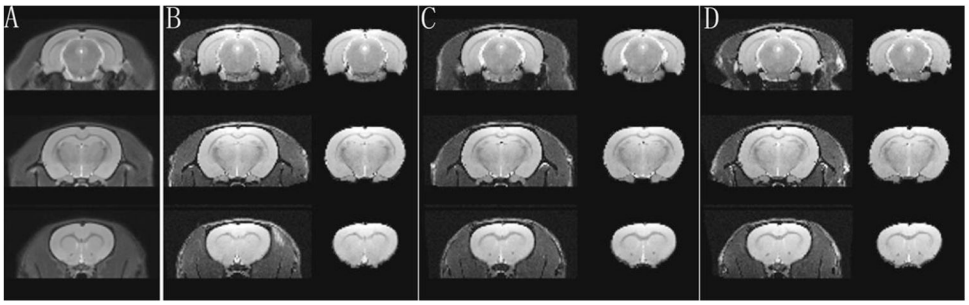

Figure 3.

The extraction results. Panel (**A**) shows three planes from the average rat brain. For randomly selected individual rats 1, 2, and 3, the registered image is shown on the left and the extracted brain tissues on the right on Panels (**B**–**D**) separately.

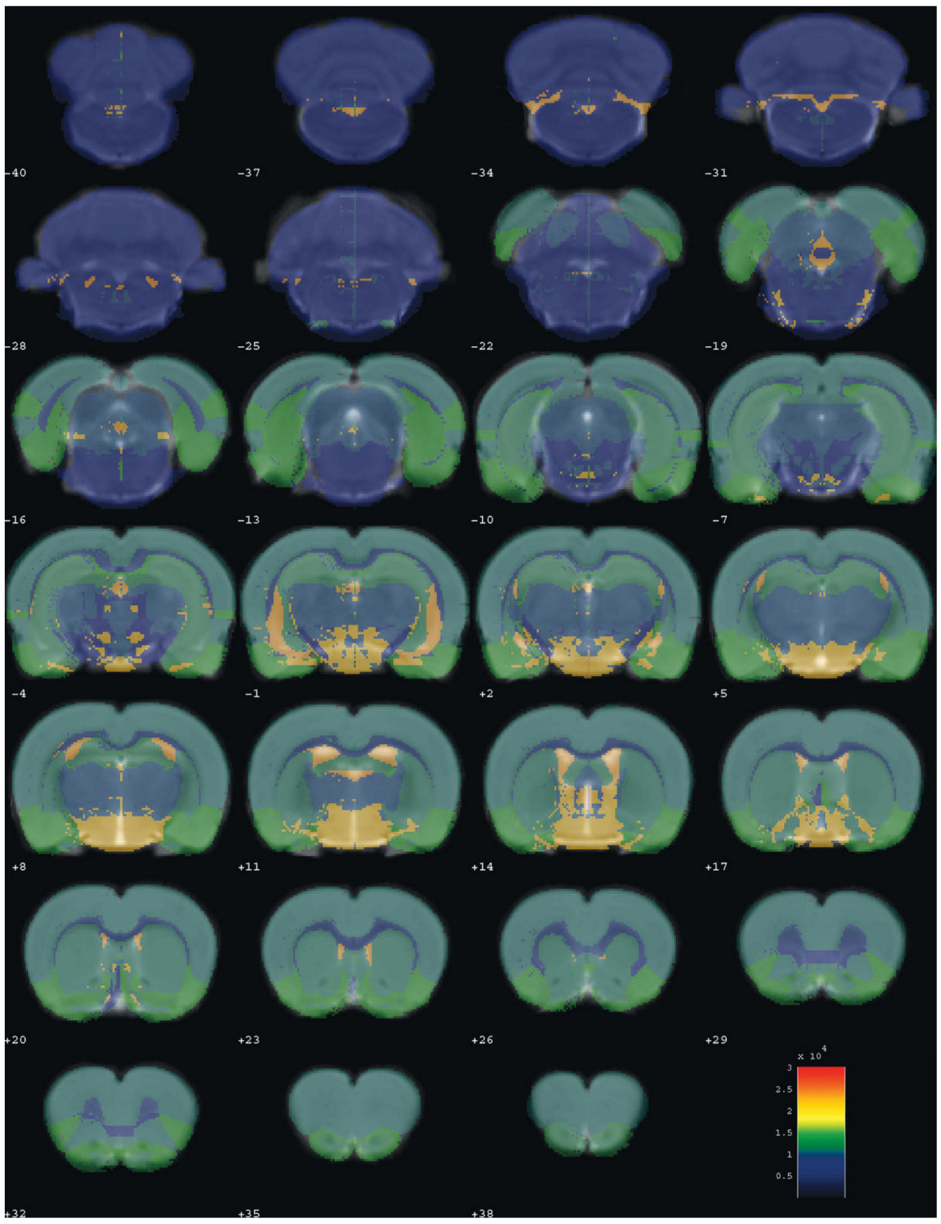

Figure 4.

Superimposing the rat brain atlas with 12 anatomical structures on the co-registered rat brain template. The rat brain atlas is presented with varying transparency and color scaled. The co-registered rat brain template is presented in gray-scale as a background. [Color figure can be viewed in the online issue, which is available at wileyonlinelibrary.com.]

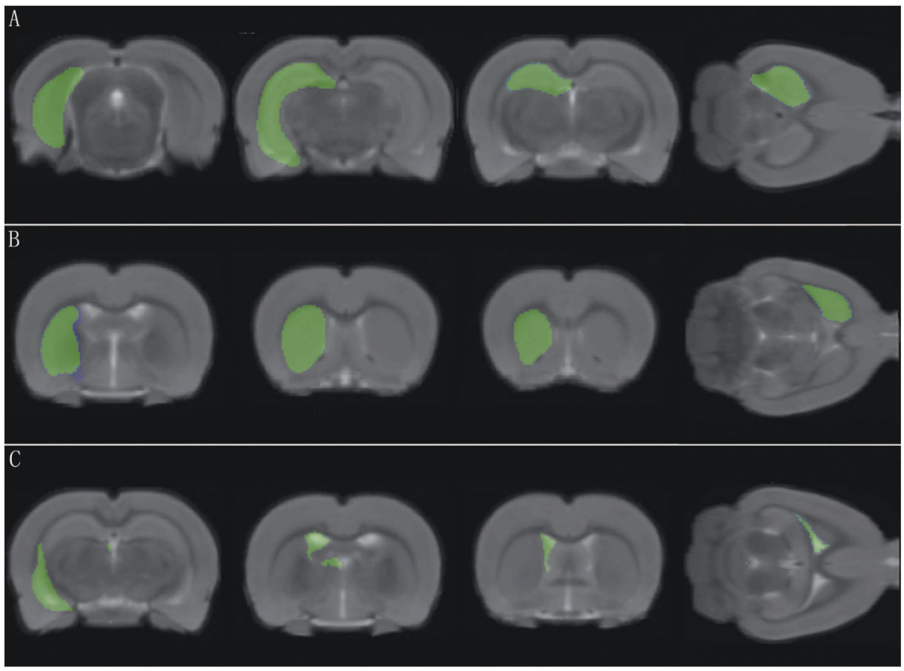

Figure 5.

Superimposing three representative anatomical structures on the co-registered rat brain template. The selected anatomical structures are extracted from the rat brain atlas and presented with varying transparency and color scaled. The co-registered rat brain template is presented in gray-scale as a background. The three selected anatomical structures are, respectively, (**A**) hippocampus, (**B**) corpus striatum, and (**C**) ventricle. [Color figure can be viewed in the online issue, which is available at wileyonlinelibrary.com.]

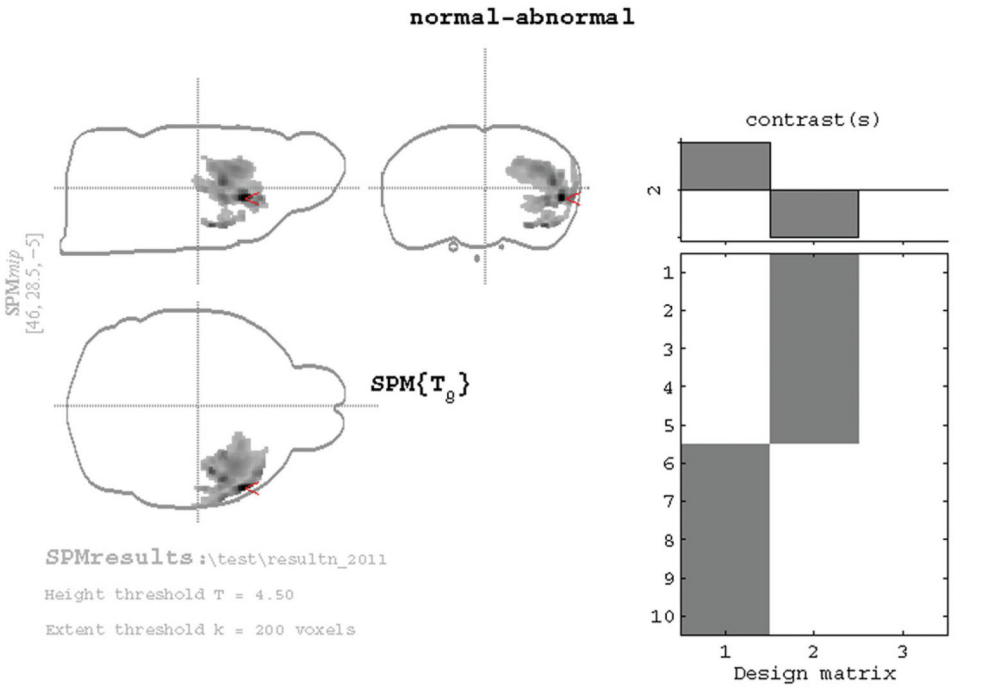

Statistics: *p-values adjusted for search volume*

cluster-level			voxel-level					x,y,z {mm}
$p_{corrected}$	k_E	$p_{uncorrected}$	$p_{FWE-corr}$	$p_{FDR-corr}$	T	(Z_e)	$p_{uncorrected}$	
0.000	4607	0.000	0.034	0.004	15.20	5.10	0.000	6 6 0
			0.256	0.014	10.50	4.53	0.000	5 9 -3
			0.262	0.014	10.44	4.52	0.000	5 5 -2

table shows 3 local maxima more than 8.0mm apart

Height threshold: T = 4.50, p = 0.001 (1.000)
Extent threshold: k = 200 voxels, p = 0.009 (0.074)
Expected voxels per cluster, <k> = 25.656
Expected number of clusters, <c> = 0.08
Expected false discovery rate, <= 0.04

Degrees of freedom = [1.0, 8.0]
Smoothness FWHM = 10.3 12.5 7.1 {mm} = 10.3 8.3 7.1 {voxels}
Search vol: 291317 cmm; 194211 voxels; 297.1 resels
Voxel size: [1.0, 1.5, 1.0] mm (1 resel = 605.89 voxels)

Figure 6.

Statistical results of reduced signals in the MCAO related regions in comparison with 10 normal controls. [Color figure can be viewed in the online issue, which is available at wileyonlinelibrary.com.]

TABLE I

Volumetric and spatial correspondence measures between the rat brain atlas and the co-registered rat brain template

	JS (%)	RV (%)	FP (%)	FN (%)
Whole brain	93.98	1.83	3.99	3.63
Right hippocampus	90.56	8.37	10.29	9.59